Phase resetting of embryonic chick atrial heart cell aggregates
Experiment and theory

John R. Clay,* Richard M. Brochu,‡ and Alvin Shrier‡
*Laboratory of Biophysics, National Institute of Neurological Disorders and Stroke, National Institutes of Health, Bethesda, Maryland 20892 USA and ‡Department of Physiology, McGill University, McIntrye Medical Building, Montreal, Quebec, Canada H3G 1Y6

ABSTRACT The influence of brief duration current pulses on the spontaneous electrical activity of embryonic chick atrial heart cell aggregates was investigated experimentally and theoretically. A pulse could either delay or advance the time of the action potential subsequent to the pulse depending upon the time in the control cycle at which it was applied. The perturbed cycle length throughout the transition from delay to advance was a continuous function of the time of the pulse for small pulse amplitudes, but was discontinuous for larger pulse amplitudes. Similar results were obtained using a model of the ionic currents which underlie spontaneous activity in these preparations. The primary ion current components which contribute to phase resetting are the fast inward sodium ion current, I_{Na}, and the primary, potassium ion repolarization current, I_{x_1}. The origin of the discontinuity in phase resetting of the model can be elucidated by a detailed examination of the current-voltage trajectories in the region of the phase response curve where the discontinuity occurs.

INTRODUCTION

Injection of a brief duration current pulse in a spontaneously beating cardiac preparation resets the phase of its rhythm (Weidmann, 1951; Jalife and Moe, 1976; Sano et al., 1978; Jalife et al., 1980; Clay et al., 1984; Van Meerwijk et al., 1984; Guevara et al., 1981, 1986). This effect depends upon both the amplitude and the timing of the pulse. For example, a depolarizing pulse applied shortly after the occurrence of the maximum diastolic potential (MDP) can significantly delay the beat subsequent to the pulse, whereas the same amplitude pulse applied at a slightly later time in the unperturbed cycle can significantly advance the time of occurrence of the next beat. This resetting of the phase of spontaneous beating can appear to be a discontinuous function of the time at which the pulse was injected, a result which has attracted considerable theoretical interest (Glass and Winfree, 1984). More dramatically, a pulse applied at a critical point in the spontaneous cycle of some cardiac preparations can stop spontaneous activity (Jalife and Antzelevitch, 1979, 1980; Gilmour et al., 1983).

The ionic mechanisms underlying these results have not been elucidated. A prerequisite for this analysis is a model of the ionic currents which underlie spontaneous activity in the particular preparation from which the activity has been observed. We recently developed such a model for embryonic chick atrial heart cell aggregates (Shrier and Clay, 1986), which is the preparation we have used in this study. These preparations beat spontaneously, even though they lack a time-dependent pacemaker current component. We have found aggregates to be particularly useful for this study, because they maintain stable, rhythmic activity in tissue culture conditions for several hours.

In the subsequent paper we have analyzed the effects of relatively low doses of tetrodotoxin (TTX) on phase resetting (Shrier et al., 1990).

Dr. Brochu's current address is Pharamacology Department, Merck-Frosst Inc., PO Box 1005, Pointe-Claire, Dorval, Quebec, Canada H9R 4P8.

Address correspondence to John R. Clay, Laboratory of Biophysics, National Institutes of Health, Building 9, Boom 1E124, Bethesda, MD 20892.

METHODS

Tissue culture techniques

The techniques used to prepare heart cell aggregates were similar to those described elsewhere (Shrier and Clay, 1986; Clay and Shrier, 1981). The atria were dissected from the hearts of White Leghorn chick embryos incubated at 37°C for 7–12 d. The tissue was enzymatically dispersed in 0.5% trypsin (1:300; Worthington Biochemical Co., Freehold, NJ) by the multiple cycle trypsinization process described by DeHaan (1967, 1970). This procedure yields a suspension consisting primarily of isolated, single cells. An inoculum of this suspension was added to an Erlenmeyer flask containing 3 ml of culture medium 818A (DeHaan, 1970) which consists, by volume, of 25% M199 (Gibco Laboratories, Grand Island, NY), 2% heat-inactivated fetal calf serum (Gibco Laboratories), and 0.5% gentamycin (Schering Corp., Bloomfield, NY) in a balanced salt solution which contained (in millimolar): NaCl, 116.0; $MgSO_4$, 0.8; NaH_2PO_4, 0.9; $CaCl_2$, 1.8; $NaHCO_3$, 26.6; glucose, 5.5; KCl, 1.3. The flask was gassed with 5% CO_2, 10% O_2, and 85% N_2, sealed with a silicone rubber stopper, and placed on a gyratory shaker for 48–72 h at 37°C. During this time spherical aggregates form with diameters usually in the 100–300-μm range (single cell diam ~15 μm). After the gyration culture procedure, the contents of the flask were

0006-3495/90/09/609/13 $2.00

transferred to a plastic tissue culture dish ($T = 37°C$). The aggregates migrated to the bottom of the dish to which they firmly adhered. In most experiments the medium was covered with a layer of mineral oil. The gas mixture given above was blown over the surface of the oil. Alternatively, the dish (0.5 ml) was perfused at a rate of 1.0 ml/min.

Electrophysiology

Electrical activity was recorded, and current pulses were injected by means of a glass microelectrode impaled within one of the cells of the aggregate. Electrode resistance was typically 50 MΩ. These results were stored for off-line analysis on a tape recorder (3964A; Hewlett-Packard Co., Palo Alto, CA) at 3¾ ips (DC-1250 Hz). The phase resetting curves in Fig. 6 were obtained from intervals measured with reference to the time when the upstroke phase of the action potential crossed 0 mV. The interval between the AP preceding a current pulse and the AP subsequent to the pulse was normalized by the control interbeat interval (IBI). Similarly, the time at which the pulse was applied was also normalized by the control IBI.

Heart cell aggregates are well suited for this study because they are space clamped based on the observation that the input conductance and capacitance of an aggregate both scale according to the size of the preparation (Clay et al., 1979). Moreover, the kinetics of the fast inward sodium ion current, I_{Na}, and the delayed rectifier potassium ion current, I_K, in aggregates appear to be identical to the kinetics of I_{Na} and I_K in single cells (Fujii et al., 1988; Clay et al., 1988).

Theory

The computer simulations given below are based upon the Shrier and Clay (1986) model of ionic currents in chick atrial heart cells. The current components are explicitly given in Table 1. The model for the inward excitatory, sodium ion current, I_{Na}, is taken from Ebihara and Johnson (1980). Inactivation of this component in their model has a single, monoexponential time course, which is consistent with recent measurements of I_{Na} from single embryonic chick heart cells (Fujii et al., 1988; A. S. Kristof and A. Shrier, unpublished results). Adult cardiac cells exhibit a more complicated time course for I_{Na} inactivation (Follmer et al., 1987). The calcium ion component, I_{Ca}, in the model is based on the measurements from chick heart cell aggregates by Josephson and Sperelakis (1982), who reported an I_{Ca} component which is activated at potentials positive to −40 mV and which is inactivated by voltage clamp steps of 200–300 ms duration. A similar component was reported by Bean (1985) in canine atrial heart cells and by Fischmeister and Hartzell (1986) in frog ventricular heart cells. The model of the delayed rectifier component, I_K, is based on the results in Shrier and Clay (1986) and Clay et al. (1988). Our analysis does not contain a transient outward potassium ion current because we have not clearly observed this component in our preparations. The primary repolarization current in the model is the potassium ion component, I_{x_1}. The description of I_{x_1} is based on the measurements in Shrier and Clay (1986). The background current, I_b, appears to consist of three components: one similar to $I_{Na,b}$ in the original McAllister et al. (1975) model of spontaneous activity in cardiac Purkinje fibers, which we have termed I_{b_1}; a component similar to the background, inwardly rectifying, potassium current, I_{K_1}, which we have termed I_{b_2}; and a third component which also inwardly rectifies, which we have termed I_{b_3}. The reversal potential for the latter current is ~−50 mV, which is also close to the reversal potential, overall for I_b. That is, I_b is in the net inward direction for $V < -50$ mV. Consequently, I_b, which is a time-independent inward current, is the essential component of the pacemaker mechanism in these cells. The experimental measurements upon which the model of I_b is based are given in Shrier and Clay (1986).

TABLE 1 Membrane current components

Sodium ion current: $I_{Na} = 90\, m^3(t)\, h(t)\, (V\text{-}40)$,

$$\dot{m}(t) = -(\alpha_m + \beta_m)m(t) + \alpha_m;\ \dot{h}(t) = -(\alpha_h + \beta_h)h(t) + \alpha_h;$$

$$\alpha_m = 320\,(V + 47.13)/\{1 - \exp[-0.1(V + 47.13)]\}\ s^{-1};$$

$$\beta_m = 80 \exp(-V/11)\ s^{-1};\ \alpha_h = 135 \exp[-(V + 80)/6.8]\ s^{-1};$$

$$\beta_h = 3{,}560 \exp(0.079\, V) + 3.1 \times 10^8 \exp[0.35(V + 3)]\ s^{-1}.$$

and $\tau_h = (\alpha_h + \beta_h)^{-1} = 0.00013\{\exp\,[-(V + 10.66)/11.1] + 1\}$ s when $V > -40$ mV

Delayed rectifier potassium current: $I_K = I_{K_0} n(t)$

$$I_{K_0} = 0.0079\, V\,[1.3\text{–}145 \exp(V/25)]/[1 - \exp(V/25)];$$

$$\dot{n}(t) = -(\alpha_n + \beta_n)\, n(t) + \alpha_n;$$

$$\alpha_n = 0.08\,(V - 15)/\{1 - \exp[-0.08(V - 15)]\}\ s^{-1};$$

$$\beta_n = 0.156 \exp[-0.055(V - 15)]\ s^{-1}.$$

Primary repolarization current: $I_{x_1} = I_o s_{x_1}(t)$

$$\dot{s}_{x_1}(t) = -(\alpha_{x_1} + \beta_{x_1})\, s_{x_1} + \alpha_{x_1};$$

$$\alpha_{x_1} = 18.4 \exp[0.12(V + 7)]\ s^{-1};$$

$$\beta_{x_1} = 0.029 \exp[-0.09(V + 7)]\ s^{-1};$$

$$I_o = 238\, y^2\,(145\, p_{x_1} - 1.3\, r_{x_1})/(1 + y + 52.8y^2),$$

with $y = 1.3\, r_{x_1}/(145\, p_{x_1})$,

$$r_{x_1} = [1 + \exp(V/25)]^{-1}, \quad \text{and} \quad p_{x_1} = 1 - r_{x_1}.$$

Background current: $I_{b_1} + I_{b_2} + I_{b_3}$, where

$$I_{b_1} = 0.034\,(V - 40),$$

$$I_{b_2} = 112.5\, y_1^3\,(145\, p_{x_1} - 1.5\, r_{x_1})/(1 + y_1 + y_1^2 + 1.5y_1^3),$$

$$I_{b_3} = 0.41\,|V + 65|\, y_2^2\,(145\, p_{x_1} - 10.7\, r_{x_1})/(1 + y_2 + 9y_2^2)$$

$$y_1 = 1.5\, r_{x_1}/(145\, p_{x_1}),\ y_2 = 10.7\, r_{x_1}/(145\, p_{x_1}).$$

Calcium ion current: $I_{Ca} = 20\, d(t)\, f(t)\, f'(t)\, (V - 30)$

$$\dot{d}(t) = -(\alpha_d + \beta_d)\, d(t) + \alpha_d;\ \dot{f}(t) = -(\alpha_f + \beta_f)\, f(t) + \alpha_f$$

$$\alpha_f = 0.025 \exp(-0.1\, V)\ s^{-1};\ \beta_f = 0.25\, V/[1 - \exp(-0.2\, V)]\ s^{-1};$$

$$\alpha_d = 2{,}600 \exp(-0.02\, V)/[\exp(-0.15\, V) + 1]\ s^{-1};$$

$$\beta_d = 1{,}780 \exp[-0.17\,(V + 39)]/\{\exp[-0.072\,(V + 39)] + 1\}\ s^{-1};$$

$$\dot{f}' = -f'[Ca_i]/(5 \times 10^{-8}) + (1 - f')/(0.025\{1 + \exp[0.10(V + 50)]\}),$$ where

$[Ca_i]$ is the internal calcium ion concentration (mol/liter), with

$$[\dot{C}a_i] = -13 \times 10^{-6}\, I_{Ca} + 80\,(10^{-7} - [Ca_i]).$$

Our model does not contain either the sodium/potassium pump current or the sodium/calcium exchange current. The close agreement between the model and the various phenomena we describe suggests that these additional mechanisms do not play a major role in phase resetting under control conditions. When aggregates are stimulated at rates faster than their spontaneous beat rate (overdrive), an ouabain-sensitive component, presumably related to the pump current, can influence both phase resetting and pacemaker activity (Zeng et al., 1990).

Computer simulation technique

The membrane potential, V, was determined from the ionic currents by numerically integrating the equation

$$dV/dt = \dot{V} = (I_{ionic} + I_{stim})/C_i, \quad (1)$$

where $I_{ionic} = I_b + I_{Na} + I_{Ca} + I_K + I_{x_1}$, I_{stim} is the externally applied stimulus current, and C_i is the input capacitance. We have used $C_i = 3.3$ nF, which is appropriate for a 130-μm diam aggregate (Clay et al., 1979).

Membrane potential changes subsequent to a given set of initial conditions were calculated from Eq. 1 using an Euler fixed-step implementation of the Rush and Larsen (1978) algorithm. An integration time step of 50 μs was routinely used for most of the results, although considerably smaller steps were used to investigate the critical region of the phase-resetting curve (Results).

RESULTS

Experimental

Basic electrophysiology

A typical recording of electrical activity from an aggregate of embryonic chick atrial cells is shown in Fig. 1 *A*. The MDP was −88 mV, the overshoot potential (OS) was 28 mV, the maximum upstroke velocity, $\dot{V}_{max}$, was 110 V/s, and the IBI was 445 ms. Pooled results for the action potential parameters were MDP = −87 ± 4 mV, OS = 23 ± 5 mV, and $\dot{V}_{max}$ = 106 ± 25 V/s (n = 5; Shrier and Clay, 1982). The model result is shown in Fig. 1 *B*. This waveform represents a limit cycle or limit trajectory. That is, the model relaxes back to the pattern of activity shown in Fig. 1 *B* after current pulse pertubations. The MDP of the model action potential is −94 mV, OS = 29 mV, $\dot{V}_{max}$ = 108 V/s, and IBI = 395 ms.

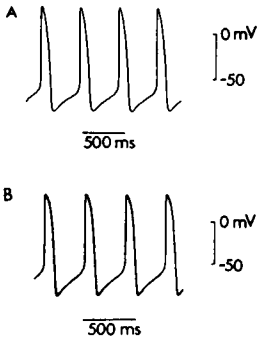

FIGURE 1 (*A*) Spontaneous electrical activity from a 130-μm diam aggregate. (*B*) Spontaneous activity predicted by the Shrier and Clay (1986) model.

A detailed comparison of the model AP with the experimental waveform is provided in Fig. 2. The experimental and theoretical results are given in Fig. 2, *A* and *B*, respectively. The two results are shown superimposed in Fig. 2 *C*. The time and voltage axes of the model result were scaled by 4% and 6%, respectively, in Fig. 3 *C* to optimize the comparison of action potential configuration. This scaling of the axes of the model AP are well within the experimentally observed variability of the AP parameters noted above. The model provides a good description of the experimental AP except for a slight discrepancy during the plateau, which was consistently observed.

Phase resetting

Examples of phase resetting are shown in Fig. 3, *A* and *C*. In this experiment a 40-nA pulse 20 ms in duration was applied close to the time of MDP in the control cycle (indicated by the time increment labeled T_1 above Fig. 3 *A*, where zero time corresponds to the 0 mV crossing on the upstroke of the action potential [AP]). The pulse produced a delay of ~30% in the time of occurrence of the subsequent AP (Fig. 3 *A*; T_2 represents the time to the AP subsequent to the pulse, where, again, zero time is from $\dot{V}_{max}$ of the upstroke of the preceeding AP. The control cycle length is represented by T_0). An AP occurred immediately after the current pulse (Fig. 3 *C*) when the pulse was applied ~1 ms later than in Fig. 3 *A*. The predictions of the model for these conditions are shown in Fig. 3, *B* and *D*, respectively. The arrow alongside the AP subsequent to the current pulse in each panel in Fig. 3 indicates the direction of phase resetting. Specifically, the arrow alongside of the AP subsequent to the pulse in Fig. 3, *A* and *B*, indicates a phase delay. The arrow pointing leftward in Fig. 3, *C* and *D*, indicates a phase advance.

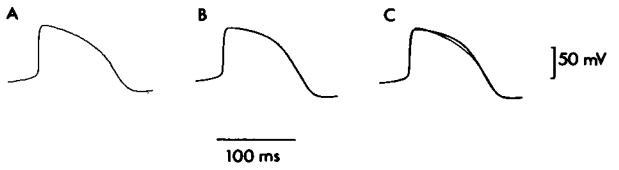

FIGURE 2 (*A*) Action potential from Fig. 1 *A* on expanded time scale. (*B*) Prediction of the model described in the text. (*C*) Superposition of the results in *A* and *B*. The time and voltage scales for the model result were scaled by 4 and 6%, respectively, to enhance this comparison.

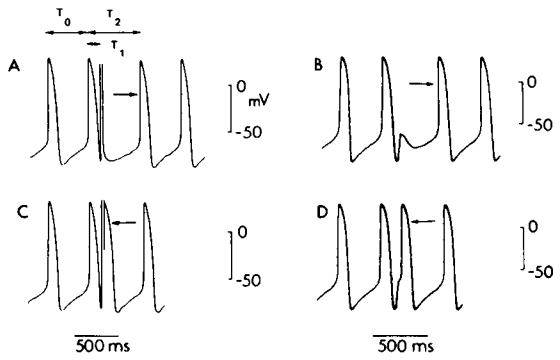

FIGURE 3 Phase resetting of rhythmic activity. (*A*) Phase delay (indicated by the arrow) caused by a 40-nA pulse 20 ms in duration applied close to the time of MDP in the control cycle. (*B*) Prediction of the model for the conditions in *A*. (*C*) Phase advance (indicated by the arrow) caused by applying the pulse ~1 ms later in the control cycle than in *A*. (*D*) Prediction of the model for the conditions in *C*. The inset above panel *A* illustrates the terminology used in the text for the control cycle length, T_0, the time of pulse application, T_1, which is measured from the time of 0 mV crossing of the upstroke of the AP preceding the pulse, and the time from the AP preceding the pulse to the AP after the pulse, T_2.

A more detailed analysis of phase resetting is shown in Fig. 4. Each column of records in Fig. 4, *A–D*, contains a control result on top and four records below in response to 20-ms current pulses of 8, 16, 32, and 48 nA amplitude for *A*, *B*, *C*, and *D*, respectively, at the times indicated by the stimulus artifacts. The smallest amplitude pulse (8 nA) produced a modest effect on the timing of the subsequent beat. The primary feature was a phase advance when the pulse was applied during the latter part of the pacemaker phase. The 16 nA pulses produced a greater effect. A clear phase delay was observed (~20% relative to the control interbeat interval) when the pulse was applied a few ms after the MDP in the control cycle. The same amplitude pulse applied 20 ms later in the cycle produced a marked phase advance. An even greater, maximal phase delay ($T_{2,max}$), ~35% relative to the control IBI, was produced with a 32 nA pulse (Fig. 4 *C*). Moreover, a 32-nA pulse applied only 1 ms later in the cycle produced a marked phase advance. The timing of the phase advance and delay was even more critical with 48 nA pulses (Fig. 4 *D*). The maximum delay produced with these pulses occurred at a time, $T_{1,max}$, which was earlier than $T_{1,max}$ for lower amplitude pulses. Moreover, $T_{2,max}$ with 48 nA pulses was $<T_{2,max}$ for 32 nA pulses, and the transition from delay to advance was more dramatic than with 32 nA pulses. The predictions of the model for all four pulse amplitudes are shown in Fig. 5, *A–D*. The model agrees well with the experimental results except for minor discrepancies. For example, the critical point in the cycle for the transition from delay to advance with the 48-nA pulses occurred a few ms after MDP in the control cycle in the model (Fig. 5 *D*), as compared with a few milliseconds before MDP in the experimental results (Fig. 4 *D*).

The phase resetting results in Figs. 4 and 5 are shown in further detail in Fig. 6, which illustrates the relative time of the beat subsequent to the current pulse stimulus (T_2/T_0) as a function of the time in the unperturbed cycle at which the pulse was applied (T_1/T_0). The current pulse amplitudes were 8, 16, . . ., 48 nA for Fig. 6, *A–F*, respectively. The intervals at which the pulses were applied in the cycle, experimentally, were incremented by 10 ms, except for the critical region of phase resetting for 32, 40, and 48 nA for which 1-ms intervals were used. The experimental results for 32–48 nA show an apparent discontinuity in that there is a sudden transition from a maximum delay to an advance without intermediate points. The model is fundamentally continuous for 32 and 40 nA, although considerably smaller time increments

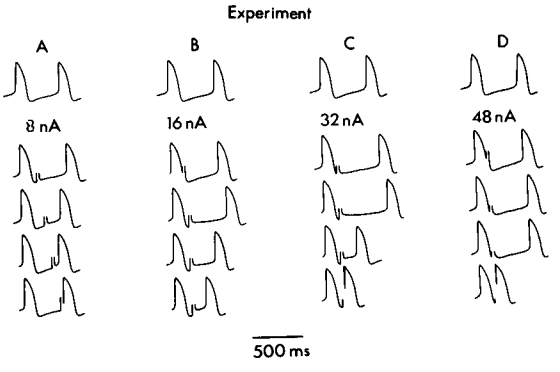

FIGURE 4 Phase resetting for 20-ms duration pulses 8, 16, 32, and 48 nA in amplitude for panels *A*, *B*, *C*, and *D*, respectively. The pulses were applied at the times indicated by the stimulus artifacts. The record at the top of each panel is a control cycle.

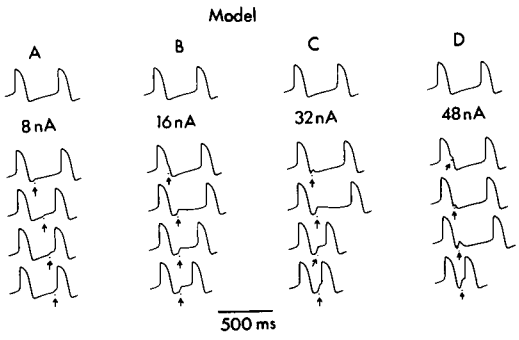

FIGURE 5 Phase resetting in the model for the conditions of Fig. 6. The horizontal bar and arrow under each record below *A*, *B*, *C*, and *D* represents the time at which the pulse was applied in the model.

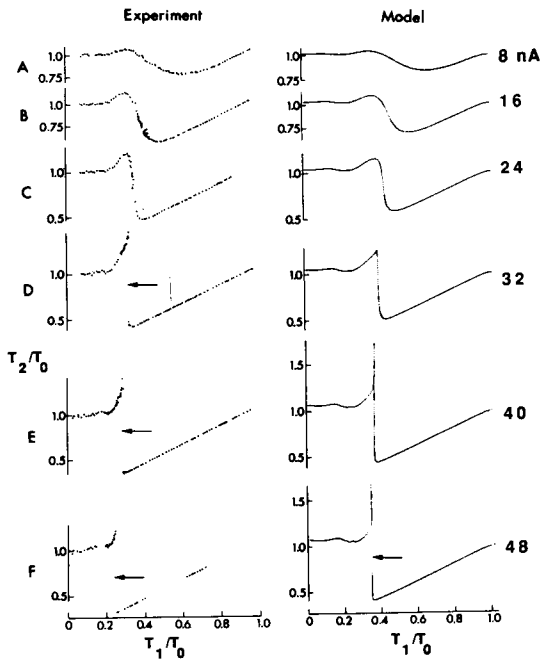

FIGURE 6 Phase-resetting curves for 8, 16, 24, 32, 40, and 48 nA pulses for *A*, *B*, *C*, *D*, *E*, and *F*, respectively. The experimental results are shown in the left panels; the theoretical results are on the right. The vertical axes represent the time from the beat before the pulse to the time of the beat subsequent to the pulse, T_2, normalized by the control IBI, T_0. (See Fig. 3 for a pictoral description of these terms.) The horizontal axes represent the times in the control cycle at which the pulses were delivered, T_1, also normalized by the control IBI.

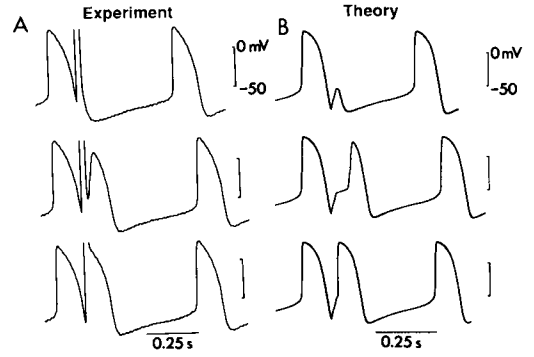

FIGURE 7 Graded response in both the experiment and model, as described in the text.

than 1 ms are required (smaller even than 1 μs for 40 nA) to see this result. (The significance and rationale of examining the model on such a fine time scale are given below [DISCUSSION].) The 48 nA phase-resetting results are discontinuous, even in the model.

Results similar to those shown above were observed in all experiments. In particular, the maximum delay observed with 20-ms duration pulses was 43 ± 8% (n = 8; ± sd). The relative point in the unperturbed cycle at which this delay occurred was 0.28 ± 0.06, which was within 10 ms, or less, of the time of occurrence of MDP in all experiments.

Graded response

The action potentials observed in this study were generally fixed events, that is, the response was all or none. However, we observed a graded response at rather high stimulus intensities, as illustrated in Fig. 7, for which 56 nA amplitude pulses were used. The top and bottom panels on Fig. 7 *A* show the apparent discontinuity in phase resetting noted above for pulses delivered ~1 ms apart. Occasionally, we observed an intermediate or graded response under these conditions, as shown in the middle panel of Fig. 7 *A*. The model mimicked these results with 70-nA pulses, as shown in Fig. 7 *B*, with pulse injection times of 107.3, 107.45, and 107.7 ms (relative to the 0 mV point on the upstroke phase of the AP), respectively, from top to bottom. The pulse for the intermediate time elicited a graded response similar to the experimental result. The significance of graded action potentials is discussed below.

Theoretical

Ionic basis of electrical activity

The ionic currents underlying the action potential are illustrated in Fig. 8. All of the currents shown below the AP of the model are scaled for a 130-μm diam aggregate, which was a typical size used in this study. The I_{Na} and I_{Ca} components contribute to the upstroke of the AP. Moreover, I_{Ca} is the sole inward current during the plateau, even though I_{Ca} inactivates completely within ~200 ms, because the AP duration of embryonic chick atrial heart cells is relatively short (~100 ms). The delayed rectifier, I_K, contributes to setting the duration of the AP, but it is a relatively minor factor during repolarization. The I_b and I_{x_1} components are the primary factors during the initial and later stages of repolarization, respectively. The I_b component rectifies significantly for $V > -20$ mV, which is reflected in the unusual profile for this current during the AP.

The mechanism of pacemaker depolarization of these cells is illustrated in Fig. 9, which shows the I_{x_1}, I_K, I_b, and I_{Na} components relative to the pacemaker phase (*top panel*), along with τ_{x_1}, the time constant for I_{x_1} gating, which is an important factor in phase resetting. The I_K component is essentially zero throughout this time. The I_{x_1} component is the only outward current from MDP to threshold. This current is offset by I_b, so that the net

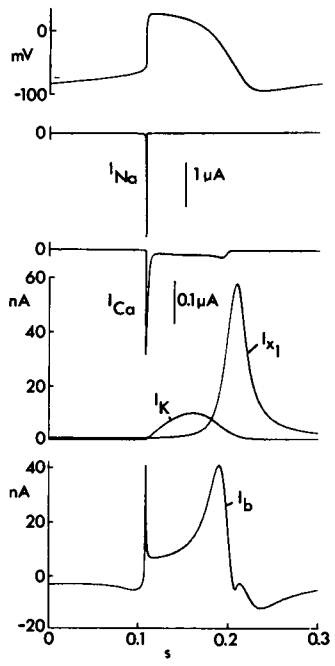

FIGURE 8 Ionic currents underlying the model action potential, as described in the text.

current, $I_{x_1} + I_b$, is inward. The I_{Na} component is a factor during the final ~50 ms of pacemaker depolarization, as in the original McAllister et al. (1975) model of pacemaker activity in cardiac Purkinje fibers. The τ_{x_1} parameter is a bell-shaped function of voltage with a peak time constant of ~1 s at −35 mV (Fig. 5 *B* of Shrier and Clay, 1986). Consequently, it increases with time during the pacemaker phase.

Ionic basis of phase resetting

The ionic mechanism of phase resetting can be elucidated by an analysis of membrane currents in the model underlying this phenomenon. The primary components are I_{Na} and I_{x_1}, as illustrated in Fig. 10. The top panel of Fig. 10 illustrates the electrical responses in the critical region of phase resetting for 32-nA pulses. The response labeled *b* corresponds to a near maximal delay in the model for these conditions. The record labeled *a* corresponds to the response in the model for a 32-nA pulse applied 3 ms later in the unperturbed cycle. The voltage changes during these two pulses essentially overlap (*arrow in top panel,* Fig. 10), because the pulses are so closely spaced. The profiles of I_{x_1} and I_{Na}, and also τ_{x_1}, during these responses are shown in the lower three panels. The dashed lines represent the time course of these components during the unperturbed pacemaker cycle, which is not shown in the top panel of Fig. 10. The effect of the pulse is to rapidly depolarize the membrane to the threshold of I_{Na}. Specifically, the pulse brings the membrane potential within range of activation of the I_{Na} window current (Attwell et al., 1979). This depolarization also increases the amplitude of I_{x_1} by increasing the

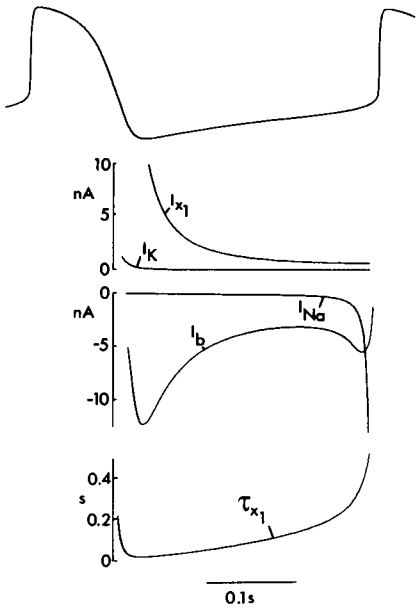

FIGURE 9 Ionic currents underlying pacemaker activity in the model. Also shown is the time course of the τ_{x_1} parameter.

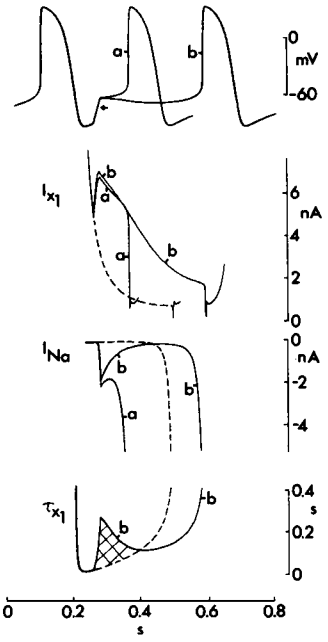

FIGURE 10 Ionic mechanism of phase advance and delay as described in the text.

driving force for potassium ions. The effect on I_{x_1} is slightly greater for record *b* because the current pulse was applied slightly earlier in the unperturbed cycle compared with record *a*. (The I_{x_1} amplitude decreases with time during the pacemaker phase as shown in Fig. 9). The net current at the end of the pulse for either *a* or *b* in Fig. 10 is nearly zero, because $-I_{x_1} \sim I_{Na} + I_b$ for these conditions. The I_b component is otherwise not a significant factor in phase resetting because it rectifies in the vicinity of the threshold (Fig. 9). That is, its amplitude is very nearly the same at the end of the pulse for either *a* or *b*. Because $I_{tot} \sim 0$ at the end of pulses in the critical range, membrane potential changes tend to occur relatively slowly after a pulse, as shown in the top panel of Fig. 10, although the relative amplitudes of I_{Na} and I_{x_1} are also factors in determining the rate of voltage change, as noted below. Moreover, the I_{x_1} time constant, τ_{x_1}, is greater for potentials close to threshold as compared with values of this variable near MDP, as shown in the bottom panel of Fig. 9. This effect is the dominant factor during a phase delay. Specifically, τ_{x_1} is rapidly changed by the current pulse from a value close to zero near MDP to ~0.4 s at the end of 32–48 nA pulses. Consequently, the I_{x_1} component remaining at the beginning of the current pulse will deactivate much more slowly than in control after the pulse, as shown by the difference between curve *b* and the dashed line (control) in the second panel of Fig. 10. This point is also illustrated by the behavior of τ_{x_1} shown in the bottom panel of Fig. 10. Specifically, the cross hatched area in this panel illustrates the time during which τ_{x_1} is greater for response *b* than in control. However, the hyperpolarizing influence of I_{x_1} is offset by the premature activation of I_{Na} near the end of these pulses, (response *a* in Fig. 10). In other words, phase resetting is, in part, a threshold effect. A current pulse applied during the pacemaker phase depolarizes the membrane to threshold of the AP, and can cause premature activation of I_{Na}, thereby advancing the phase of the rhythm. Moreover, the pulse can lead to a phase delay if it is insufficient to activate I_{Na} because of the increase in I_{x_1} described in Fig. 10. This analysis provides a ready explanation for the leftward shift and increased steepness of the phase resetting curve with larger pulse amplitudes (Fig. 6). The critical point in phase resetting is determined by a trade-off between I_{Na} and I_{x_1}. (The I_b component is very nearly the same at the end of pulses in the critical range, as noted above). A larger amplitude pulse drives the membrane potential to the I_{Na} threshold at earlier times in the cycle, which shifts the critical point leftward. Moreover, a larger pulse produces a relatively greater enhancement of I_{x_1}. Consequently, a large pulse which does not elicit an AP will result in a relatively large phase delay near the critical point. The transition in the phase response curve at the critical point is steeper at greater pulse amplitudes because there is a trade-off between a more pronounced (premature) activation of I_{Na} and a larger I_{x_1}.

Phase plane analysis

Further insight into this problem, in particular the apparent discontinuity of phase resetting (Fig. 6), can be obtained by plotting the membrane potential, V, as a function of the net ionic current (I_{ionic} in Eq. 1). This analysis is illustrated for the model in Fig. 11. This I–V plot describes a cycle, a limit cycle, which is traversed for each electrical cycle (pacemaker phase and the AP) of the preparation. Technically, the limit cycle is a curve in a multidimensional space described by the membrane potential, V, and all the gating variables, such as m and h for I_{Na}, and n for I_K. However, the gating variables are solely functions of V and time, t. Moreover, the membrane potential over any time increment is determined by the net ionic current (Eq. 1). Consequently, the I–V phase plot is likely to illustrate the general features of the problem. The arrows on the plot in Fig. 11 indicate the direction of time. The dominant current components at various points in the control cycle are also indicated. The small symbol (●) indicated by the arrow within the cycle represents the equilibrium point ($I_{ionic} = 0$, which occurs at $V \sim -51$ mV). That is, the equilibrium point occurs at the membrane potential for which the steady-state current is zero, as illustrated by the intersection between the dashed line and the voltage axis in the inset in Fig. 11. This point is unstable, in the model, which is consistent with experimental observations. We were not able to stop spontaneous activity with brief current pulses. Moreover, the preparation resumed spontaneous activity after it had

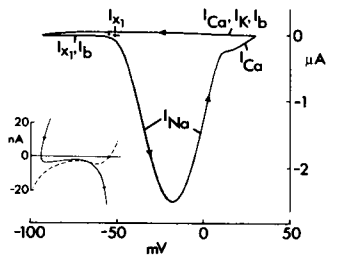

FIGURE 11 Current-voltage trajectory of the model as described in the text. The ordinate is the net ionic current, I_{ionic}, during spontaneous activity as a function of potential. The arrows indicate the direction of time. The dominant current components at various phases of the cycle are indicated by the labels. (*Inset*) Part of the limit cycle corresponding to the latter part of repolarization and the pacemaker phase on expanded current scale. The dashed line is the steady-state current voltage relation. The crossing of the voltage axis by this relation is indicated both in the inset and above (●).

been held at the equilibrium point in voltage clamp conditions.

The I–V phase plane analysis of current pulse perturbations is illustrated in Figs. 12 and 13 for 16, 24, 32, and 40 nA (Fig. 12, *A–D*, respectively) and 44 and 48 nA pulses (Fig. 13, *A* and *B*, respectively). Only a portion of the unperturbed limit cycle is shown in these results, consisting of the latter part of repolarization and the pacemaker phase, as in the inset of Fig. 11. These are the portions of the control cycle for which a current pulse has the greatest effect. The voltage responses corresponding to these trajectories are shown in the insets above each panel. These results straddle the transition from phase delay to phase advance. That is, some of these trajectories correspond to phase advances, whereas others correspond to phase delays, as illustrated by the insets. The dashed lines in Figs. 12 and 13 illustrate the I–V trajectories during the 20-ms duration pulses themselves. These lines essentially superimpose for 40, 44, and 48 nA (they nearly do so for 32 nA, Fig. 12 *C*) because the times at which these pulses were delivered in the control cycle are closely spaced. For example, the pulses for 32 nA were delivered at 153.5, 154.25, 154.35, and 154.5 ms (relative to the time of the 0 mV crossing on the upstroke phase of the AP) for traces 1, 2, 3, and 4, respectively. That is, the times for all four results fall within a range of 1 ms, which is just beyond the level of resolution, experimentally. Phase resetting for these conditions appears to be discontinuous, experimentally, as illustrated in Fig. 6 *D*. However, this process is clearly continuous in the model (Fig. 6 *D*, *right hand panel*) and Fig. 12 *C*.

The timing in the region of maximal delay is even more critical for 40 nA (Fig. 12 *D*). The five different results shown here correspond to a 10-μs range near the 143 ms point in the unperturbed cycle. The traces are labeled according to the times at which the pulses were injected in the model. These results begin to superimpose upon one another, an effect which is shown more clearly in Fig. 13. This line of trajectories defines a border between two different types of response. For example, trajectory 5 in Fig. 12 *D* corresponds to the pulse which was applied later in the unperturbed cycle than the other four responses. Consequently, slightly more of the I_{Na} component is activated at the end of the pulse in this case, as compared with the other four cases, which is sufficient to carry the model beyond threshold of the AP. Trajectory 4 corresponds to a slightly earlier time (1 μs earlier) of pulse injection compared with trajectory 5. Slightly less of the I_{Na} component is available at the end of the pulse in this case. Consequently, the I_{x_1} component has the greater effect, and the membrane potential begins to move in the hyperpolarizing direction. The amount of activatable I_{Na}

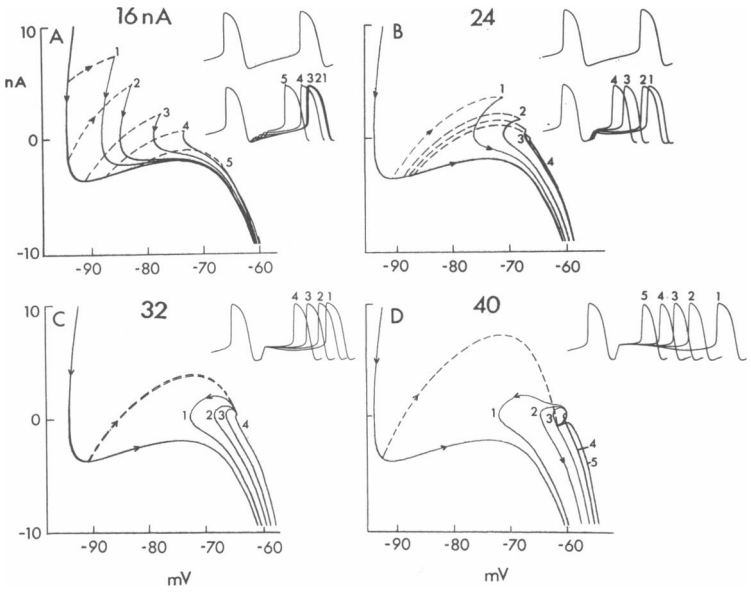

FIGURE 12 Current-voltage phase plane description of phase resetting. Each panel contains a portion of the control current-voltage trajectory, as in the inset of Fig. 11, along with 4 or 5 trajectories produced by 20-ms duration current pulses of amplitude 16, 24, 32, and 40 nA for panels *A*, *B*, *C*, and *D*, respectively. The dashed lines represent the trajectories during the current pulses, themselves. These trajectories superimpose, essentially, in panels *C* and *D*, because the times of pulse injection are so closely spaced. The arrows on the trajectories indicate the direction of time. The full voltage responses corresponding to each trajectory are shown in the inset of each panel. The control result is shown in the top part of this inset in panels *A* and *B*. The control interbeat interval (IBI) is 395 ms. The two voltage marks to the left of the records in the insets represent 0 and −50 mV, respectively. The symbol (●) in panel *D* represents the equilibrium point at ~ −51 mV.

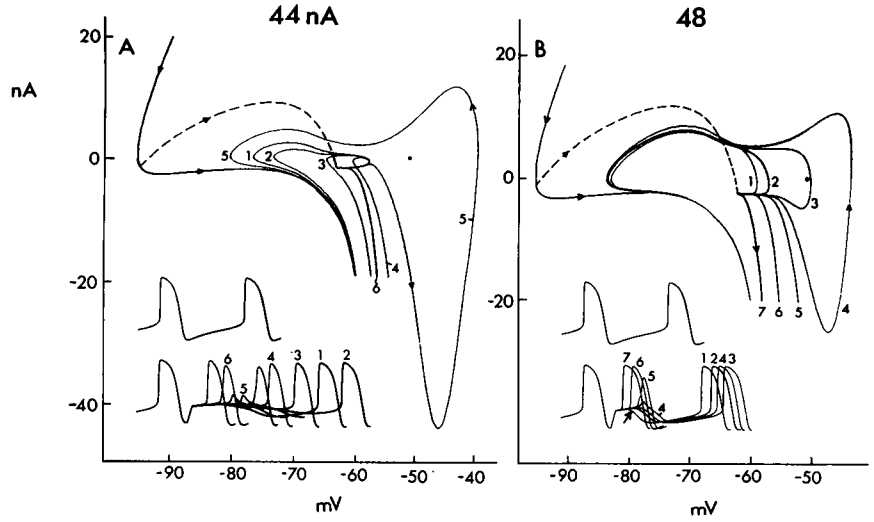

FIGURE 13 Phase plane description of current pulse perturbations for 44 and 48 nA, panels *A* and *B*, respectively. The arrows indicate the direction of time. The symbol (●) indicates the equilibrium point at ~ −51 mV. The inset below the trajectories in each panel contains the full voltage responses themselves. The arrow in the inset of *B* indicates the first maximum after the current pulse for trajectory 1.

for both trajectories 4 and 5 is reduced relative to the normal AP, because I_{Na} inactivation increases during the time that the system remains in the region of threshold. This effect is evident by comparing the AP for trajectories 4 and 5 with the AP for trajectory 1. The $\dot{V}_{max}$ and the AP duration of trajectories 4 and 5 are both reduced, as will be discussed in greater detail in the following paper. Nevertheless, the phase resetting effect is clearly continuous in the model for 40 nA, as also shown in Fig. 6, although the time scale over which the continuity occurs is well beyond the range of experimental resolution, because of noise sources, both extrinsic and intrinsic to the preparation (see below).

The line of threshold trajectories after the current pulse is more clearly defined for 44 and 48 nA (Fig. 13), as noted above. The position of this line is slightly different for each of these cases, as compared with Fig. 12 *D*, because the initial conditions differ (time of pulse injection; difference primarily in the initial condition of the I_{x_1} gating variable s_{x_1}). However, the pattern of the trajectories for 44 nA is similar to that of the 40-nA results, including, for example, the turning back of trajectory 5 upon itself. The effect of I_{Na} inactivation is greater in this case, because the membrane potential at the end of the pulses is further depolarized than it is in the 40-nA results. In fact, sodium current inactivation is so great that it prevents initiation of a full-blown AP. A markedly graded response occurs, in the model, as exemplified by trace 5 in Fig. 13 *A*. (Note that trace 5, which appears as a small "hump" in the inset, actually traverses a greater range in the I–V plot because of the current scale. The full upstroke of traces 1–4 and 6 are not shown in the phase space representation. We also note that the turning back of trajectories 1–4 upon themselves corresponds to a subthreshold oscillation of the membrane potential, which is especially evident in trajectory 2.) The question of continuity of phase resetting for trace 5 is ambiguous. For example, phase resetting is discontinuous if 0 mV is (arbitrarily) defined as the event marker, whereas it actually is continuous if −40 mV is defined as the event marker. This problem of event identification does not arise for 48 nA. Phase resetting in this instance is clearly discontinuous, no matter how the event marker is defined. Moreover, the pattern of trajectories is different than that of the 40- and 44-nA results. In particular, no trajectories turn back upon themselves because a greater amount of I_{x_1} remains at the end of the pulse than with the lower amplitude pulses. That is, the membrane potential is sufficiently depolarized at the end of the pulse so that it actually is in the lower end of the I_{x_1} activation curve. Consequently, once the system turns away from the threshold in the hyperpolarizing direction, it will continue in that direction to ~ −80 mV before I_{x_1} is sufficiently deactivated to allow the inward background current to resume depolarization (as in the control cycle). A level of −80 mV is sufficiently negative to allow normal reactivation of I_{Na} to occur. Conversely, trajectories which move away from the threshold in the depolarizing direction will result in a full-blown AP, provided the system does not linger in the vicinity of threshold (trace 6). The longer the system moves along the line of trajectories after the pulse, the more graded the response will be. Both the amplitude

and the time of the initial voltage maximum after the pulse are continuous functions of the time at which the pulse is applied, t_{pulse}, which is apparent in the inset of Fig. 13 *B*. However, the first voltage maximum after the pulse for trajectories 1 and 2 (indicated by the arrow for trace 1) can, in no manner, be thought of as action potentials. The first AP in these cases occurs approximately one cycle after the pulse, whereas the first AP for trajectory 5, for example, corresponds to the first voltage maximum after the pulse. Consequently, the time of the first AP is a discontinuous function of t_{pulse}, regardless of how the event marker is defined.

DISCUSSION

The above analysis demonstrates that the issue of the continuity of the phase resetting curve is closely related to the threshold phenomenon, specifically the apparent "all-or-none" threshold, which was a key issue for membrane physiologists throughout the first half of this century (Cole et al., 1955). Indeed, one of the first questions to be asked of the Hodgkin and Huxley (1952) model of the nerve action potential was, "Does the model have a true 'all-or-none' threshold, i.e., a threshold which is a discontinuous function of stimulus parameters?" Cole et al. (1955), who were the first to analyze the Hodgkin and Huxley (1952) model on a digital computer, concluded that it did possess true "all-or-none" behavior. Fitzhugh (1955) immediately challenged this conclusion, on purely theoretical grounds, by showing that the model did not possess a saddle equilibrium point, a necessary requirement for all-or-none behavior. Fitzhugh and Antosiewicz (1959) later showed that Cole et al. (1955) had made a technical error in their calculations, which led to an apparent "all-or-none" result, and that the response of the Hodgkin and Huxley (1952) model was, fundamentally, a graded, or continuous function of stimulus parameters, although the continuity was apparent only at a level of 1 part in 10^8, or less (Clay, 1977), far below the resolution achievable experimentally. Nevertheless, these results proved to be more than an academic exercise, because they ultimately led to the discovery of a graded, or continuous, response in nerve membrane under some experimental conditions (Cole et al., 1970). The surprising outcome of our analysis is that phase resetting in an ionic model is, fundamentally, a discontinuous process for some experimental conditions. (This result is predicted for a limit cycle oscillator, on purely theoretical grounds, by the analysis of Kawato [1981].) Our analysis also shows that the reason for this result lies in a key difference between the threshold problem and the phase-resetting problem. The threshold of our model is, fundamentally, a continuous function of pulse parameters, because it does not contain a saddle equilibrium point. (As a counterexample, our model of embryonic chick ventricular heart cell aggregates does possess such a feature under certain conditions [Clay et al., 1984].) Consequently, the model predicts that the action potential should be graded under some pulse amplitudes, as demonstrated experimentally in Fig. 7. Graded responses have also been observed in other cardiac preparations (Weidmann, 1955; Jalife and Moe, 1979; Guevara et al., 1986). Phase resetting is a continuous function of pulse parameters, fundamentally, for relatively small, as well as moderately large, pulse amplitudes, although the continuity in the latter case is difficult to observe experimentally. However, phase resetting is discontinuous both experimentally and in the model for pulse amplitudes which are large relative to the net ionic current during the latter part of repolarization and during pacemaking. These pulses produce significant inactivation of I_{Na}, which effectively inhibits the development of full-blown AP's, thereby causing the preparation to skip a beat, essentially, before resuming full-scale spontaneous activity.

Comparison with circle model analysis

The phase-resetting problem has attracted considerable theoretical interest (cf. Glass and Winfree, 1984, for a review), as the above material suggests. Much of this work is based on a simple two parameter model possessing a limit cycle, represented by a circle with an equilibrium point at its center. A current pulse in this model instantaneously shifts, or transforms, the unperturbed limit cycle, C, to a new limit cycle, C'. Moreover, the perturbed cycle is assumed to relax instantaneously back to the unperturbed cycle at the end of the pulse. This scheme predicts two distinct types of phase resetting; one which is a smoothly continuous function of the time of injection of the pulse, t_{pulse}, so called Type 1, and a second type, Type 0, which is a discontinuous function of t_{pulse}. The perturbed cycle, C', is assumed to encompass the equilibrium point for Type 1 resetting (small amplitude pulses), whereas it does not encompass the equilibrium point in Type 0 resetting (large amplitude pulses). That is, the model predicts the existence of a discrete transition between the two types of phase resetting, which is inconsistent with our analysis (Fig. 13 *A*)

We have attempted to draw a further parallel between this approach and the ionic current model in Fig. 14. All four panels in Fig. 14 contain the control current-voltage trajectory of the model, curve *a*, which is also shown in Fig. 11. This trajectory can, in global terms, be thought of as a circle encompassing an equilibrium point at its center

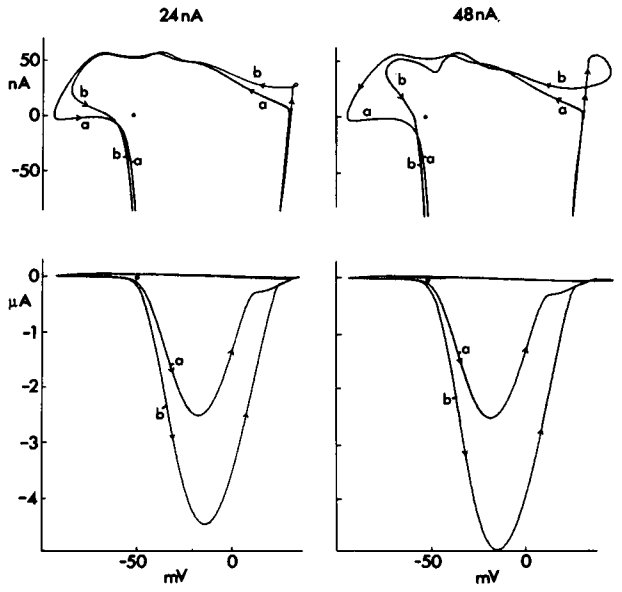

FIGURE 14 Transformed current-voltage trajectory analysis. Curve *a* in the left- and right-hand panels is the control current-voltage trajectory, as in Fig. 11. Curve *b* in the left-hand panel represents the transformed, or mapped, trajectory for 24 nA current pulses 20 ms in duration. That is, each point of *b* represents the current and the voltage at the end of pulses beginning at each point of curve *a*. Curve *b* in the right hand panel describes the same analysis for 48 nA pulses. The top portion on each side represents part of curves *a* and *b* on an expanded current scale. Note that curve *b* in both cases encompasses the equilibrium point. Moreover, curve *b* is effectively shifted leftward by these depolarizing current pulses. This result comes about because I_{Na} is normally inactivated, to an extent, during the unperturbed pacemaker phase. Consequently, a current pulse applied near MDP of the unperturbed cycle which elicits an AP will result in a greater activation of I_{Na} than in control.

($V \sim -51$ mV). The transformed cycles for 20-ms duration pulses of 24 and 48 nA amplitudes are shown in the left and right hand panels of Fig. 14, respectively (labeled *b*). That is, curves *b* represent the I–V plots at the end of pulses starting from all points of the control cycle. Phase resetting is clearly continuous for 24-nA pulses both experimentally and theoretically, whereas it is discontinuous for 48 nA in both cases, as illustrated in Fig. 6. However, the perturbed or transformed cycle in both cases encompasses the equilibrium point (see Fig. 14 legend) in contrast to the circle model analysis (Fig. 4 in Glass and Winfree, 1984). This comparison cannot be too closely drawn, because the ionic model contains several variables, whereas the circle model is strictly a two variable model. Nevertheless, the analysis in Fig. 14 reflects some essential differences between the two approaches. A phase delay in the circle model is caused by moving the phase point instantaneously to an earlier point in the unperturbed cycle relative to 0 mV on the upstroke phase of the AP. However, the ionic model does not instantaneously return to the limit cycle during a phase delay. In fact, the delay essentially corresponds to the time which the model takes to return to the limit cycle. In other words, the relaxations of the ionic model to the limit cycle after a current pulse contain time-dependent features which are not contained in the circle model.

General significance

Most, if not all, membrane oscillators have an inward current, either I_{Na} or I_{Ca}, or both, and a time-dependent outward current of some type usually carried by potassium ions. This component invariably has a bell-shaped voltage dependence to its gating parameter which decreases with hyperpolarization in the pacemaker voltage range. The mechanism of a phase advance and a phase delay would be the same in such a mechanism as in our analysis. For example, a sufficiently large current pulse will cause premature activation of the inward component thereby leading to a phase advance. A pulse which fails to produce this effect will lead to a phase delay because the time constant of the outward current will have been shifted by the pulse to a larger value. Specific models in the literature to which this analysis is applicable are the Yanagihara et al. (1980) model of the sino-atrial node, which has both an I_{Na} and an I_{Ca} component as in our model, and an I_K component which is similar to our description of I_{x_1}. Similarly, the more recent DiFrancesco and Noble (1985) model of pacemaker activity in cardiac Purkinje fibers also has an I_K component which is similar to the description of I_{x_1} in the original McAllister et al. (1975) model. Our model does not contain the time-dependent pacemaker current, I_f, because we did not find this component in the pacemaker potential range. Models of the s-a node include this component (Yanagihara et al., 1980; Noble and Noble, 1984; Noble et al., 1989), although its role is unclear. Nathan (1987) has proposed that it is not a significant factor based on voltage clamp measurements from rabbit s-a nodal cells. His view is that pacemaking is attributable to the background inward current in conjunction with the decay of outward, repolarizing, potassium current, which is similar to the mechanism of pacemaking in our preparations (Shrier and Clay, 1986). The I_f component is also not a significant factor in the Noble and Noble (1984) model under normal conditions. For example, Noble et al. (1989) have shown that the removal of I_f from the Noble and Noble (1984) model changes the interbeat interval by only 7% (Fig. 6 of Noble et al., 1989). The background, inward current is the pacemaker component under these conditions, as in our model.

Comparison with other work

Relatively few theoretical studies of phase resetting in ionic current models have been reported in the literature. Best (1979), Reiner and Antzelevitch (1985), Chay and Lee (1984, 1985), and Guevara and Shrier (1987) have carried out analyses similar to ours in, respectively, the Hodgkin and Huxley (1952) model of squid axons with a bias current to produce repetitive activity, the Bristow and Clark (1982) model of spontaneous activity in the sinus node, the Beeler and Reuter (1977) model of the ventricular myocardium made to fire repetitively with a current bias, and the McAllister et al. (1975) model of spontaneous activity in cardiac Purkinje fibers. Best (1979) has emphasized the importance of investigating these models on an exceedingly fine time scale, as we have also done, and Guevara and Shrier (1987) have emphasized graded AP's, which we also feel is an important feature of the phase-resetting problem. Reiner and Antzelevitch (1985) have emphasized the role of the pacemaker current, I_f, in relatively long phase delays in the s-a node. This component is not a factor in our analysis. We have not observed I_f in the pacemaker voltage range in atrial cells (Shrier and Clay, 1982, 1986; Clay et al., 1988). Moreover, the I_f component is not a factor in our theoretical analysis, as noted above. We agree with Reiner and Antzelevitch (1985) that a time-dependent component with slow kinetics (relative to the I_{Na} kinetics) is required to obtain relatively long phase delays (30–50%). The I_{x_1} component fulfills this role in our analysis. This current is not activated in the steady state in the −90 to −60-mV range. However, it transiently flows during the latter phase of repolarization and the initial phase of pacemaker depolarization. Consequently, it can play a significant role after a current pulse applied during these portions of the control cycle.

As noted above, several experimental observations of phase resetting in cardiac preparations have been reported. Of these Van Meerwijk et al. (1984) and Guevara et al. (1986) are the most relevant to our work because their results were also obtained from aggregates of chick embryonic heart cells. In particular, we note that Van Meerwijk et al. (1984) reported a discrete transition between Type 1 and Type 0 phase resetting and they also emphasized an all-or-none character of the AP. However, a close examination of their experimental records, in particular Fig. 6 of their paper, indicates that the electrical response in their hands was also graded. As noted above, the graded response implies that the transition between continuous and discontinuous phase resetting cannot be precisely defined.

We gratefully acknowledge Michael Guevara and John Rinzel for helpful discussions, and Laurie Sehn for technical assistance in some experiments.

This work was supported by grants to Dr. Shrier from the Quebec Heart and Stroke Foundation and the Medical Research Council of Canada.

Received for publication 5 January 1990 and in final form 2 May 1990.

Note added in proof: Recently, M. C. Sanguinetti and N. K. Jurkiewicz (*J. Gen. Physiol.* In press) have reported a repolarization current from guinea-pig ventricular myocytes which is remarkably similar to our I_{x_1} results. They have labeled this component I_{Kr}.

REFERENCES

Attwell, D., I. Cohen, D. Eisner, M. Ohba, and C. Ojeda. 1979. The steady-state TTX-sensitive ("window") sodium current in cardiac Purkinje fibers. *Pfluegers Arch. Eur. J. Physiol.* 379:137–142.

Bean, B. P. 1985. Two kinds of calcium channels in canine atrial cells. Differences in kinetics, selectivity, and pharmacology. *J. Gen. Physiol.* 86:1–30.

Beeler, G. W., and H. Reuter. 1977. Reconstruction of the action potential of ventricular myocardial fibres. *J. Physiol. (Lond.).* 268:177–210.

Best, E. N. 1979. Null space in the Hodgkin-Huxley equations. A critical test. *Biophys. J.* 27:87–104.

Bristow, D. G., and J. W. Clark. 1982. A mathematical model of primary pacemaking cells in the SA node of the heart. *Am. J. Physiol.* 243:H207–H218.

Chay, T. R., and Y. S. Lee. 1984. Impulse responses of automaticity in the Purkinje fiber. *Biophys. J.* 45:841–849.

Chay, T. R., and Y. S. Lee. 1985. Phase resetting and bifurcation in the ventricular myocardium. *Biophys. J.* 47:641–651.

Clay, J. R. 1977. Monte Carlo simulation of membrane noise: an analysis of fluctuations in graded excitation of nerve membrane. *J. Theor. Biol.* 64:671–680.

Clay, J. R., and A. Shrier. 1981. Analysis of subthreshold pacemaker currents in chick embryonic heart cells. *J. Physiol. (Lond.).* 312:471–490.

Clay, J. R., L. J. DeFelice, and R. L. DeHaan. 1979. Current noise parameters derived from voltage noise and impedance in embryonic heart cell aggregates. *Biophys. J.* 28:169–184.

Clay, J. R., M. R. Guevara, and A. Shrier. 1984. Phase resetting of the rhythmic activity of embryonic heart cell aggregates. Experiment and theory. *Biophys. J.* 45:699–714.

Clay, J. R., C. E. Hill, D. Roitman, and A. Shrier. 1988. Repolarization current in embryonic chick atrial heart cells. *J. Physiol. (Lond.).* 403:525–537.

Cole, K. S., H. A. Antosiewicz, and P. Rabinowitz. 1955. Automatic computation of nerve excitation. *J. SIAM.* 3:153–172.

Cole, K. S., R. Guttman, and F. Bezanilla. 1970. Nerve membrane excitation without threshold. *Proc. Natl. Acad. Sci. USA.* 65:884–891.

DeHaan, R. L. 1967. Regulation of spontaneous activity and growth of embryonic chick heart cells in tissue culture. *Dev. Biol.* 16:216–249.

DeHaan, R. L. 1970. The potassium sensitivity of isolated embryonic heart cells changes with development. *Dev. Biol.* 23:226–240.

DiFrancesco, D., and D. Noble. 1985. A model of cardiac electrical activity incorporating ionic pumps and concentration changes. *Philos. Trans. R. Soc. Lond. B.* 307:353–398.

Ebihara, L., and E. A. Johnson. 1980. Fast sodium current in cardiac muscle. A quantitative description. *Biophys. J.* 32:779–790.

Fischmeister, R., and H. C. Hartzell. 1986. Mechanism of action of acetylcholine on calcium current in single cells from frog ventricle. *J. Physiol. (Lond.).* 376:183–202.

Fitzhugh, R. 1955. Mathematical models of threshold phenomena in the nerve membrane. *Bull. Math. Biophys.* 17:257–278.

Fitzhugh, R., and H. A. Antosiewicz. 1959. Automatic computation of nerve excitation. Detailed corrections and additions. *J. SIAM.* 7:447–458.

Follmer, C. H., R. E. Ten Eick, and J. Z. Yeh. 1987. Sodium current kinetics in cat atrial myocytes. *J. Physiol. (Lond.).* 384:169–197.

Fujii, S., R. Ayer, and R. L. DeHaan. 1988. Development of the fast sodium current in early embryonic chick heart cells. *J. Membr. Biol.* 101:209–233.

Gilmour, R. F., Jr., J. J. Heger, E. N. Prystowsky, and D. P. Zipes. 1983. Cellular electrophysiologic abnormalities of diseased human ventricular myocardium. *Am. J. Cardiol.* 51:137–144.

Glass, L., and A. T. Winfree. 1984. Discontinuities in phase-resetting experiments. *Am. J. Physiol.* 246:R251–R258.

Guevara, M. R., and A. Shrier. 1987. Phase resetting in a model of cardiac Purkinje fiber. *Biophys. J.* 52:165–175.

Guevara, M. R., L. Glass, and A. Shrier. 1981. Phase locking, period-doubling bifurcations, and irregular dynamics in periodically stimulated cardiac cells. *Science (Wash. DC).* 214:1350–1353.

Guevara, M. R., A. Shrier, and L. Glass. 1986. Phase resetting of spontaneously beating embryonic ventricular heart cell aggregates. *Am. J. Physiol.* 251:H1298–H1305.

Hodgkin, A. L., and A. F. Huxley. 1952. A quantitative description of membrane current and its application to conduction and excitation in nerve. *J. Physiol. (Lond.).* 117:500–544.

Jalife, J., and G. K. Moe. 1976. Effect of electrotonic potentials on pacemaker activity of canine Purkinje fibers in relation to parasystole. *Circ. Res.* 39:801–808.

Jalife, J., and C. Antzelevitch. 1979. Phase resetting and annihilation of pacemaker activity in cardiac tissue. *Science (Wash. DC).* 206:695–697.

Jalife, J., and G. K. Moe. 1979. A biologic model of parasystole. *Am. J. Cardiol.* 43:761–772.

Jalife, J., and C. Antzelevitch. 1980. Pacemaker annihilation: diagnostic and therapeutic implications. *Am. Heart J.* 100:128–130.

Jalife, J., A. J. Hamilton, V. R. Lamanna, and G. K. Moe. 1980. Effects of current flow on pacemaker activity of the isolated kitten sinoatrial node. *Am. J. Physiol.* 238:H307–H316.

Josephson, I., and N. Sperelakis. 1982. On the ionic mechanism underlying adrenergic-cholinergic antagonism in ventricular muscle. *J. Gen. Physiol.* 79:69–86.

Kawato, M. 1981. Transient and steady-state phase response curves of limit cycle oscillators. *J. Math. Biol.* 12:13–30.

McAllister, R. E., D. Noble, and R. W. Tsien. 1975. Reconstruction of the electrical activity of cardiac Purkinje fibers. *J. Physiol. (Lond.).* 251:1–59.

Nathan, R. D. 1987. Role of I_f in pacemaker activity of the sinoatrial node. *Biophys. J.* 51:263*a*. (Abstr.)

Noble, D., and S. J. Noble. 1984. A model of sino-atrial node electrical activity based on a modification of the DiFrancesco-Noble (1984) equations. *Proc. R. Soc. B.* 222:295–304.

Noble, D., D. DiFrancesco, and J. Denyer. 1989. Ionic mechanism in normal and abnormal cardiac pacemaker activity. *In* Neuronal and Cellular Oscillators J. W. Jacklet, editor. Marcel Dekker, Inc., New York. 59–85.

Reiner, V. S., and C. Antzelevitch. 1985. Phase resetting and annihilation in a mathematical model of sinus node. *Am. J. Physiol.* 249:H1143–H1153.

Rush, S., and H. Larsen. 1978. A practical algorithm for solving dynamic membrane equations. *IEEE (Inst. Electr. Electron. Eng.) Trans. Biomed. Eng.* 25:389–393.

Sano, T., T. Sawanobori, and H. Adaniya. 1978. Mechanism of rhythm determination among pacemaker cells of the mammalian sinus node. *Am. J. Physiol.* 235:H379–H384.

Shrier, A., and J. R. Clay. 1982. Comparison of the pacemaker properties of chick embryonic atrial and ventricular heart cells. *J. Membr. Biol.* 69:49–56.

Shrier, A., and J. R. Clay. 1986. Repolarization currents in embryonic chick atrial heart cell aggregates. *Biophys. J.* 50:861–874.

Shrier, A., J. R. Clay, and R. M. Brochu. 1990. Effects of tetrodotoxin on the spontaneous activity of embryonic chick atrial heart cell aggregates. Phase resetting and annihilation of activity with current pulses. *Biophys. J.* 58:623–629.

Van Meerwijk, W. P. M., G. deBruin, A. C. G. VanGinneken, J. VanHartevelt, H. J. Jongsma, E. W. Kruyt, S. S. Scott, and D. L. Ypey. 1984. Phase resetting properties of cardiac pacemaker cells. *J. Gen. Physiol.* 83:613–629.

Weidmann, S. 1951. Effect of current flow on the membrane potential of cardiac muscle. *J. Physiol. (Lond.).* 115:227–236.

Weidmann, S. 1955. Effect of the cardiac membrane potential on the rapid availability of the sodium-carrying system. *J. Physiol. (Lond.).* 127:213–224.

Yanagihara, K., A. Noma, and H. Irisawa. 1980. Reconstruction of Sino-atrial node pacemaker potential based on the voltage clamp experiments. *Japn. J. Physiol.* 30:841–857.

Zeng, W.-Z., L. Glass, and A. Shrier. 1990. Evolution of rhythms during periodic stimulation of embryonic chick heart cell aggregates. *PACE.* 13:263*a*. (Abstr.)